Localised land-use and maize agriculture by the pre-Columbian Casarabe Culture in Lowland Bolivia

Article

Supplemental Material

Supplementary Information

Methods

Core Photographs

High resolution line scan images were taken of the sediment core from *Laguna Loma Suarez* (LLS) using a Geotek Multi Sensor Core Logger (MSCL) Core Imaging System at the British Ocean Core Sediment Research Facility (BOSCORF). The resulting images were calibrated using a reference card of known colour images under the same conditions as the sediment.

Quantitative Colour Data

Supporting quantitative colour data were obtained from the core, at 0.5 cm stratigraphic resolution, using a Konica Minolta 2600d spectrophotometer mounted on a Geotek MSCL Core Workstation at BOSCORF. This device registers colour in absolute red, green, and blue (RGB) intensities, as well as in the L*a*b* system defined by the Commission Internationale de l'Éclairage (CIELAB). This system records lightness (L*) from 0 (black) to 100 (white), the green-red spectrum (a*, red = positive, green = negative) and the blue-yellow spectrum (b*, yellow = positive, blue = negative), and is particularly useful for the detection of minor changes in colour (Rogerson et al., 2006).

Magnetic susceptibility

Magnetic susceptibility analysis was undertaken at 0.5 cm resolution on both overlapping cores using a Bartington point sensor mounted on a MSCL Core Workstation. These measurements were collected at the same time as the aforementioned colour data.

Laboratory Code	Sample Identifier (depth below sediment/water interface, cm)	Conventional 14C age (BP ± 1σ)	% Yield	δ13CVPDB‰ ±0.1	Outlier?	Calibrated date (BCE/CE)	Calibrated date (yr CE ±2σ)	
							From	To
OxA-X-3233-26	LLS 15-15.5	-405 ± 18	62.0	-27.2112	N	Modern	Modern	
OxA-X-3254-18	LLS-22.0-23.0	-295 ± 17	43.4	-25.7729	N	Modern	Modern	
OxA-X-3254-19	LLS-26.5-27.5	752 ± 18	59.5	-24.0058	N	1327 ± 55	1272	1382
OxA-X-3209-32	LLS 30.5-31.5	1141 ± 59	50.8	-21.9448	N	906 ± 134	772	1028
OxA-X-3254-20	LLS-30.5-31.5-1	1352 ± 18	47.4	-20.3374	N	721 ± 53	668	774
OxA-X-3254-24	LLS-34.0-35.0	1525 ± 18	55.8	-19.2516	N	591 ± 47	544	638
OxA-X-3233-27	LLS 43-44	707 ± 19	70.3	-22.96	Y	1338 ± 50.5	1287	1388
OxA-X-3254-25	LLS-46.0-47.0	-298 ± 17	44.3	-25.5554	Y	Modern	Modern	
OxA-X-3233-28	LLS 49-50	247 ± 19	81.0	-24.8042	Y	1725 ± 75	1650	1800
OxA-X-3254-26	LLS-49.0-50.0-1	2189 ± 19	69.3	-20.1638	Y	-229 ± 123	-354	-107
OxA-X-3254-27	LLS-54-55	1550 ± 18	52.0	-20.1938	N	581 ± 53	528	634
Beta-612306	LLS 60.5-61.0	1270 ± 30	/	-20.4	N	787 ± 99	688	886
OxA-X-3238-35	LLS 69-70	1614 ± 18	54.2	-18.6465	N	482 ± 60	435	542
Beta-579660	LLS 80.5-81.5	2400 ± 30	/	-18.4	N	-472.5 ± 261	-734	-211

Table SI: Conventional and calibrated radiocarbon dates for samples obtained from LLS, calibrated using the SHCal20 calibration curve (Hogg et al.*, 2020). Bayesian radiocarbon age models are available for this record within the Supplementary Information (Figs. S1 and S2). Calibrated age range follows 95.4% CI.*

Supplementary Figures

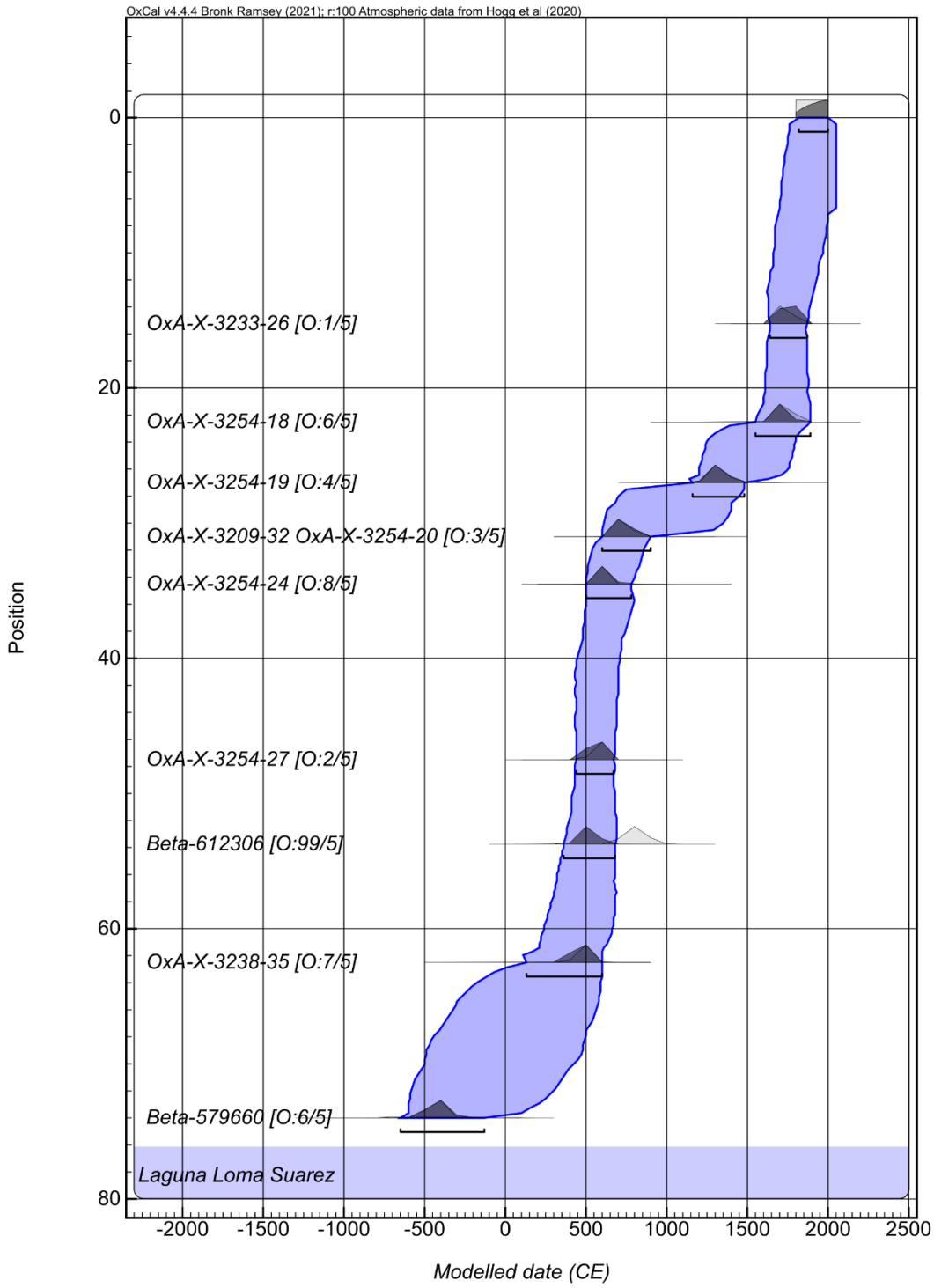

Figure S1: Bayesian age-depth model for LLS. This graph excludes the sedimentary unit between 43 and 50 cm, as well as its associated dates. This model is built from 10 AMS 14C dates calibrated to the SHCal20 curve (Bronk Ramsey, 2009; Hogg et al.*, 2020). Brackets beneath each age estimate show 95.4% CI. Outlier analysis output is noted as 'O: posterior probability/prior probability'.*

The following code was used to produce this Bayesian age-depth model:

```
Options()
 {
  Resolution=100;
 };
 Plot()
 {
  Curve("SHCal20","shcal20.14c");
  Outlier_Model("General",T(5),U(0,4),"t");
  P_Sequence("Laguna Loma Suarez",1,2,U(-2,2))
  {
   Boundary();
   R_Date("Beta-579660", 2400, 30)
   {
    Outlier("General", 0.05);
    z=74;
   };
   R_Date("OxA-X-3238-35", 1614, 18)
   {
    Outlier("General", 0.05);
    z=62.5;
   };
   R_Date("Beta-612306", 1270, 30)
   {
    Outlier("General", 0.05);
    z=53.75;
   };
   R_Date("OxA-X-3254-27", 1550, 18)
   {
    Outlier("General", 0.05);
    z=47.5;
   };
   R_Date("OxA-X-3254-24", 1525, 18)
   {
    Outlier("General", 0.05);
    z=34.5;
   };
   R_Combine("OxA-X-3209-32 OxA-X-3254-20")
   {
    R_Date("OxA-X-3254-20", 1352, 18);
    R_Date("OxA-X-3209-32", 1141, 59);
    Outlier("General", 0.05);
    z=31;
   };
   R_Date("OxA-X-3254-19", 725, 18)
   {
    Outlier("General", 0.05);
    z=27;
   };
   R_Date("OxA-X-3254-18", Top_Hat(1900,100))
   {
    Outlier("General", 0.05);
    z=22.5;
   };
   R_Date("OxA-X-3233-26", Top_Hat(1900,100))
   {
    Outlier("General", 0.05);
    z=15.25;
   };
   Boundary(Top_Hat(1900,100))
   {
    z=0;
   };
  };
 };
```

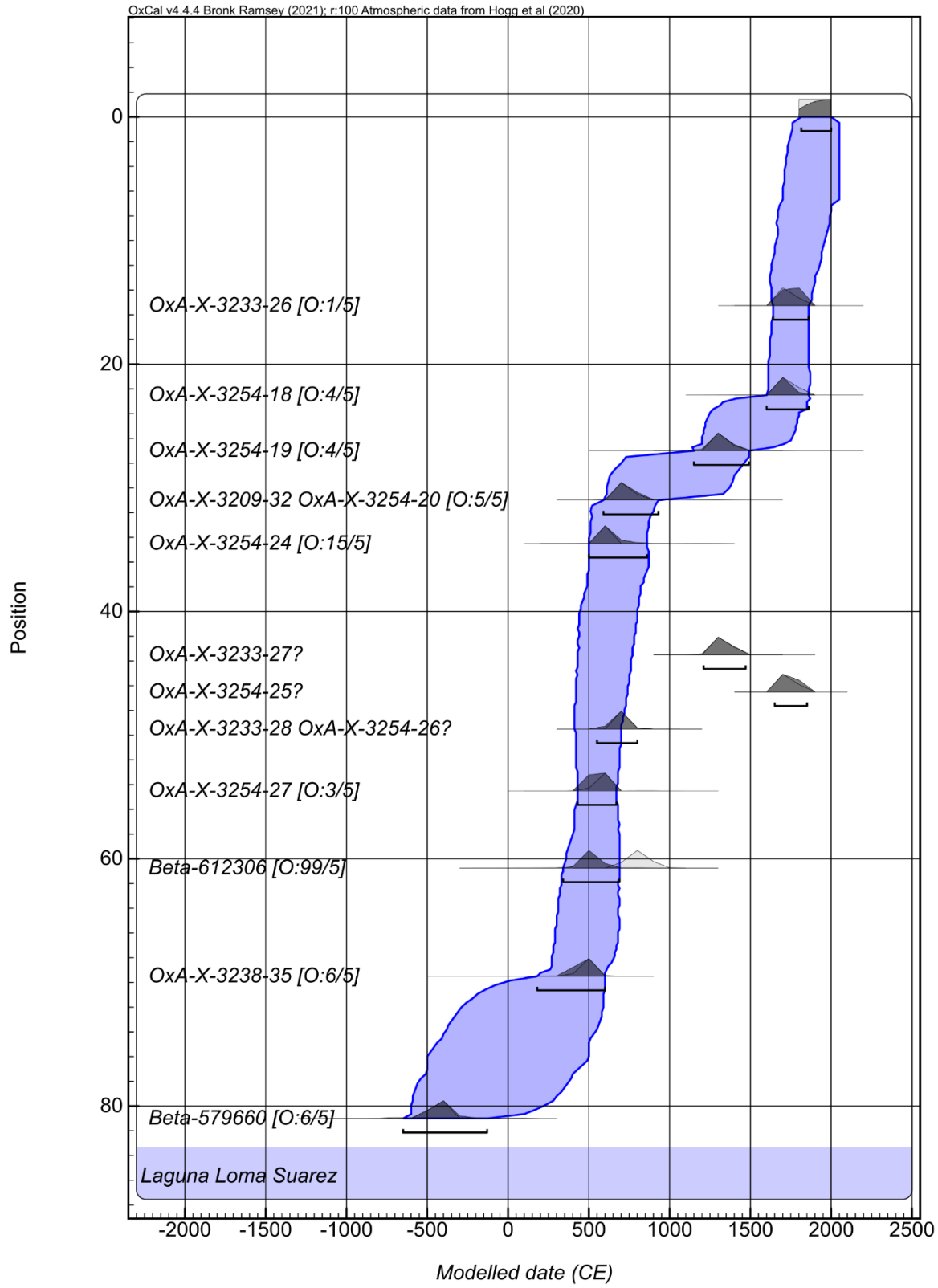

Figure S2: Bayesian age-depth model for LLS. This graph includes the sedimentary unit between 43 and 50 cm, as well as its associated dates. This model is built from 10 AMS ^{14}C dates calibrated to the SHCal20 curve (Bronk Ramsey, 2009; Hogg et al.*, 2020). Brackets beneath each age estimate show 95.4% CI. Outlier analysis output is noted as 'O: posterior probability/prior probability'.*

The following code was used to produce this Bayesian age-depth model:

```
Options()
 {
  Resolution=100;
 };
 Plot()
 {
  Curve("SHCal20","shcal20.14c");
  Outlier_Model("General",T(5),U(0,4),"t");
  P_Sequence("Laguna Loma Suarez",1,2,U(-2,2))
  {
   Boundary();
   R_Date("Beta-579660", 2400, 30)
   {
    Outlier("General", 0.05);
    z=81;
   };
   R_Date("OxA-X-3238-35", 1614, 18)
   {
    Outlier("General", 0.05);
    z=69.5;
   };
   R_Date("Beta-612306", 1270, 30)
   {
    Outlier("General", 0.05);
    z=60.75;
   };
   R_Date("OxA-X-3254-27", 1550, 18)
   {
    Outlier("General", 0.05);
    z=54.5;
   };
   R_Combine("OxA-X-3233-28 OxA-X-3254-26")
   {
    R_Date("OxA-X-3254-26", 2189, 19);
    R_Date("OxA-X-3233-28", 247, 19);
    Outlier();
    z=49.5;
   };
   R_Date("OxA-X-3254-25", Top_Hat(1900,100))
   {
    Outlier();
    z=46.5;
   };
   R_Date("OxA-X-3233-27", 707, 19)
   {
    Outlier();
    z=43.5;
   };
   R_Date("OxA-X-3254-24", 1525, 18)
   {
    Outlier("General", 0.05);
    z=34.5;
   };
   R_Combine("OxA-X-3209-32 OxA-X-3254-20")
   {
    R_Date("OxA-X-3254-20", 1352, 18);
    R_Date("OxA-X-3209-32", 1141, 59);
    Outlier("General", 0.05);
    z=31;
   };
   R_Date("OxA-X-3254-19", 725, 18)
   {
    Outlier("General", 0.05);
    z=27;
   };
   R_Date("OxA-X-3254-18", Top_Hat(1900,100))
   {
    Outlier("General", 0.05);
    z=22.5;
   };
   R_Date("OxA-X-3233-26", Top_Hat(1900,100))
```

```
  {
   Outlier("General", 0.05);
   z=15.25;
  };
  Boundary(Top_Hat(1900,100))
  {
   z=0;
  };
 };
};
```

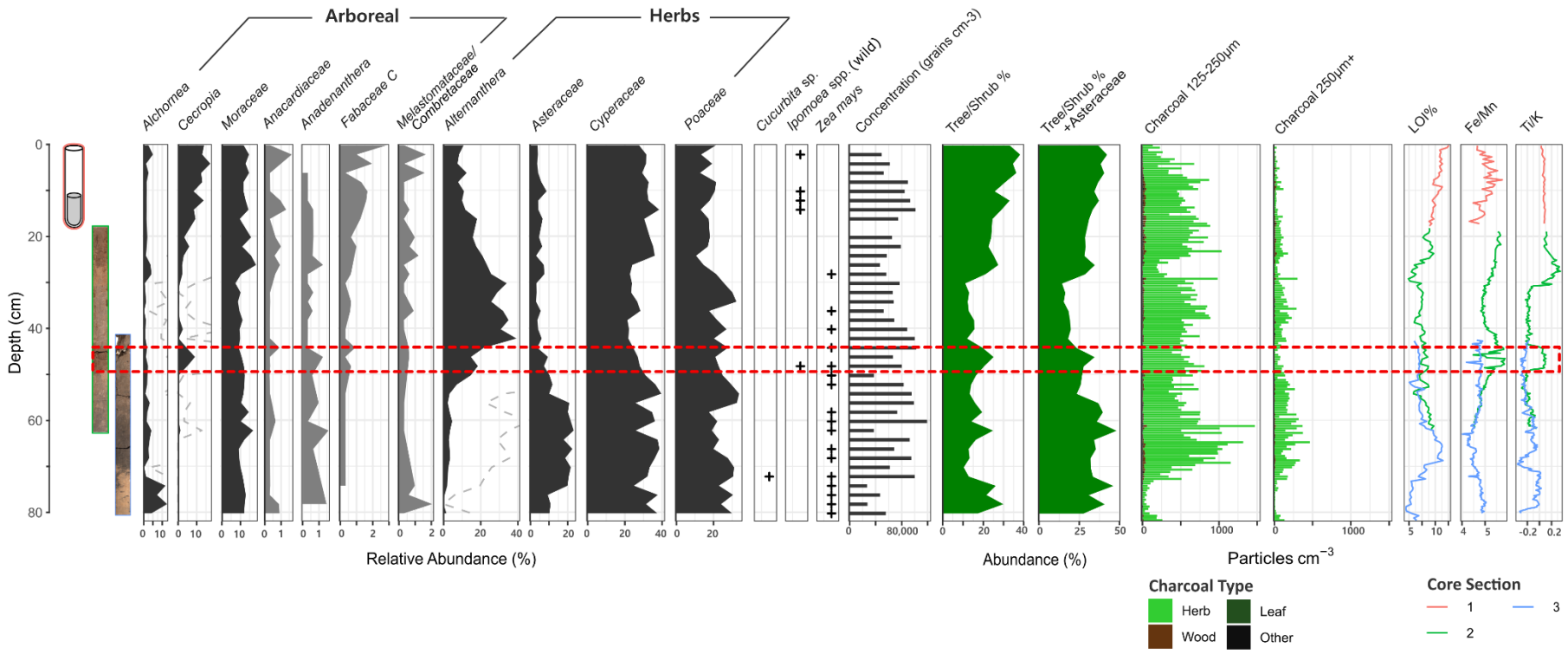

Figure S3: Summary pollen percentage diagram for LLS plotted against depth, alongside charcoal and geochemical data. Pollen percentages are relative to the total terrestrial pollen sum. Crosses denote presence/absence of cultigen pollen grains of Zea mays, Cucurbita and Ipomoea sp., which have been concentrated using the methodology of Whitney et al. (2012). *Dashed curves denote x10 exaggerations of certain key pollen taxa. The horizontal red dotted lines highlight the 7 cm section of sediment core removed from the main summary pollen diagram.*

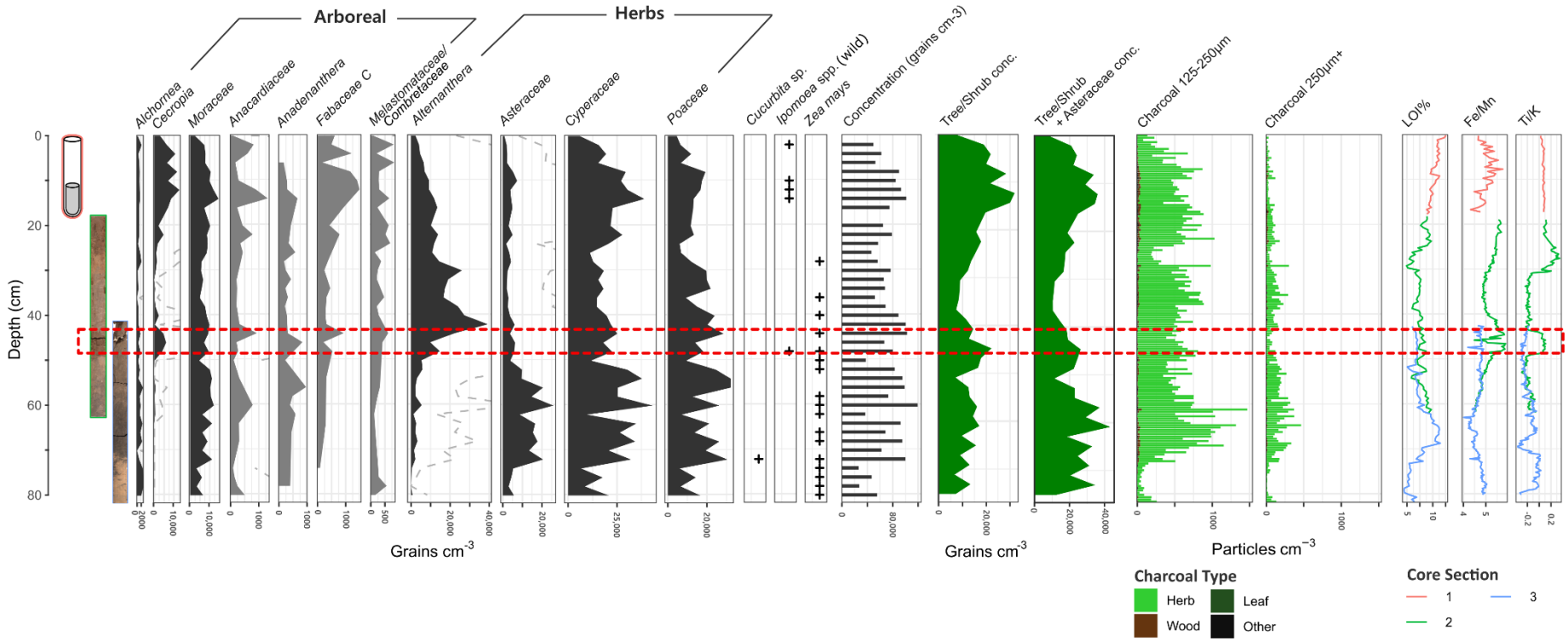

Figure S4: Summary pollen concentration diagram for LLS plotted against depth, alongside charcoal and geochemical data. Crosses denote presence/absence of cultigen pollen grains of Zea mays, Cucurbita and Ipomoea sp., which have been concentrated using the methodology of Whitney et al. (2012). *Dashed curves denote x10 exaggerations of certain key pollen taxa. The horizontal red dotted lines highlight the 7 cm section of sediment core removed from the main summary pollen diagram.*

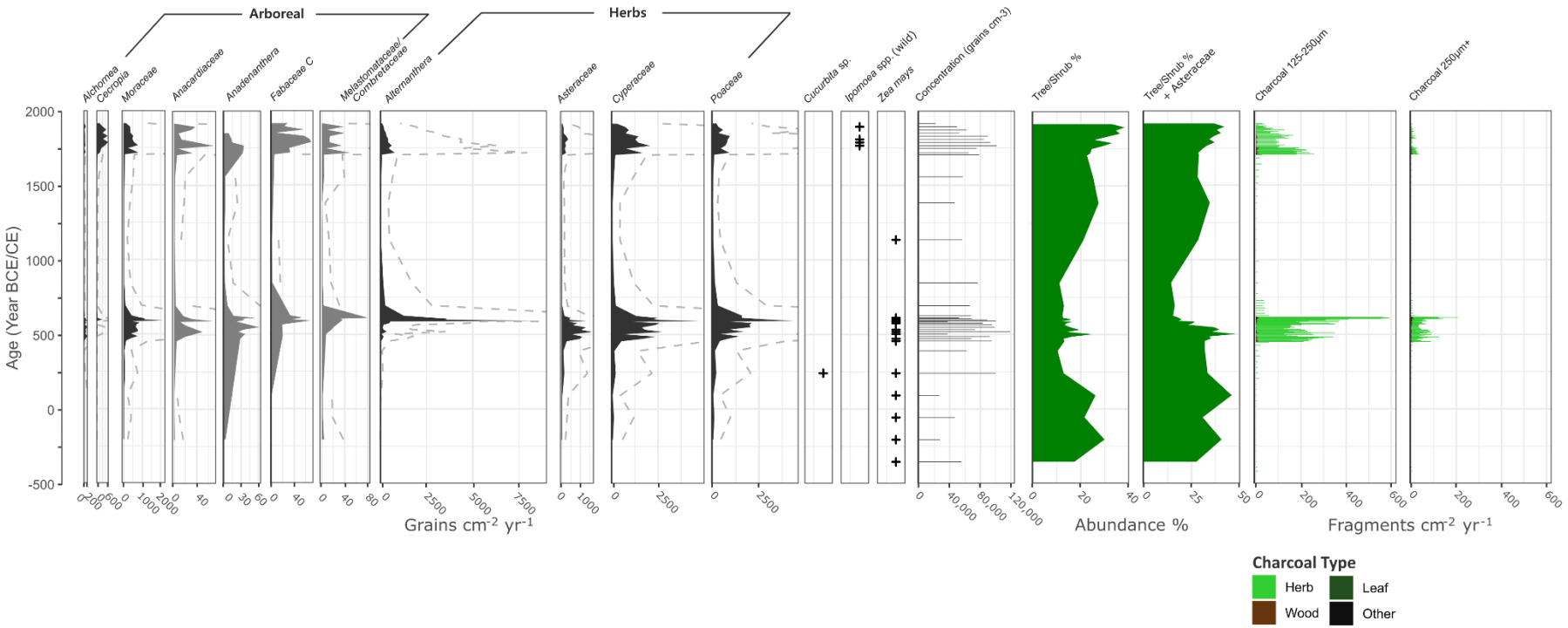

Figure S5: Summary pollen accumulation rate (PAR)/influx diagram for LLS plotted against age, alongside charcoal and geochemical data. Crosses denote presence/absence of Zea mays, Cucurbita, and Ipomoea sp. grains concentrated using the methodology of Whitney et al. (2012). *Dashed curves denote x10 exaggerations.*

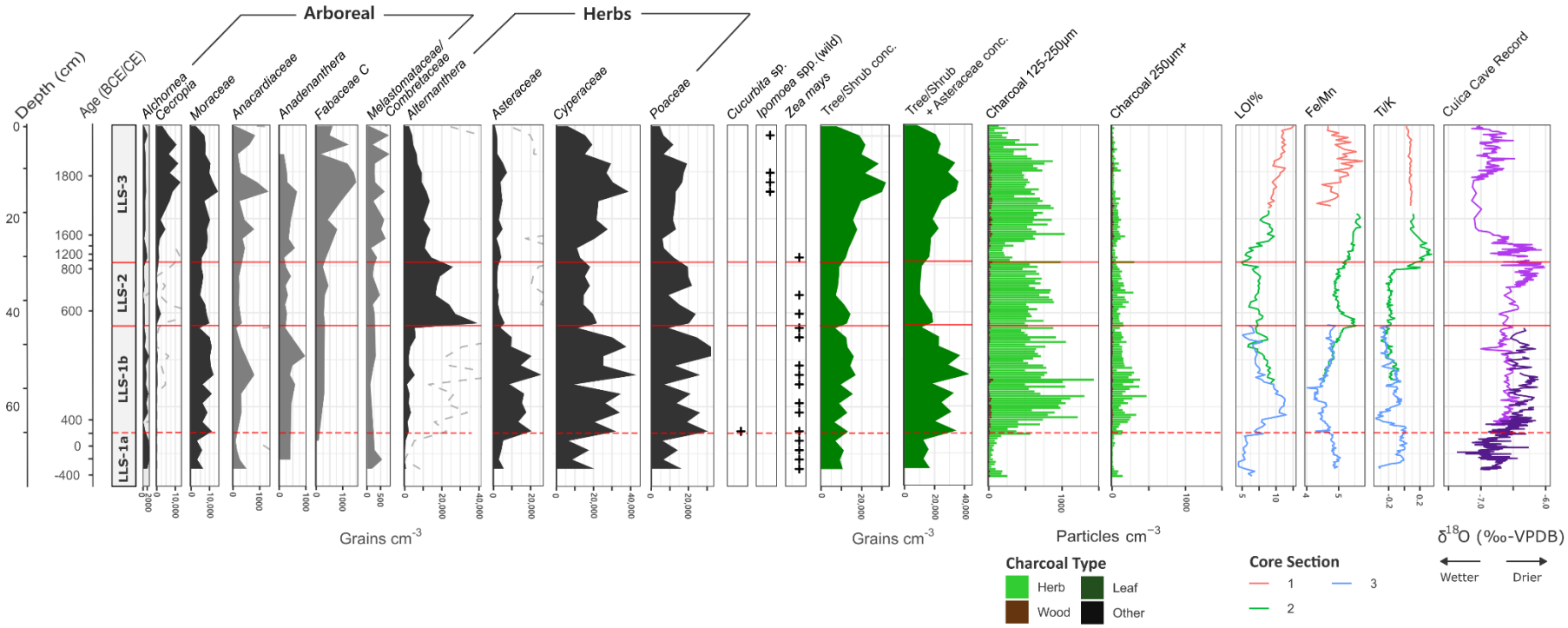

Figure S6: Summary pollen concentration diagram of key pollen types at LLS plotted against depth, alongside charcoal and geochemical data, as well as *the $\delta^{18}O$ speleothem record from Cuica cave* (Libera et al., 2022). Crosses denote presence/absence data for *Zea mays*, Cucurbita, and Ipomoea sp. grains concentrated using the methodology of Whitney et al., (2012). *Dashed curves denote x10 exaggerations of certain key pollen taxa. The diagram has been zoned based on the results of a CONISS agglomerative clustering algorithm applied to pollen taxa.*

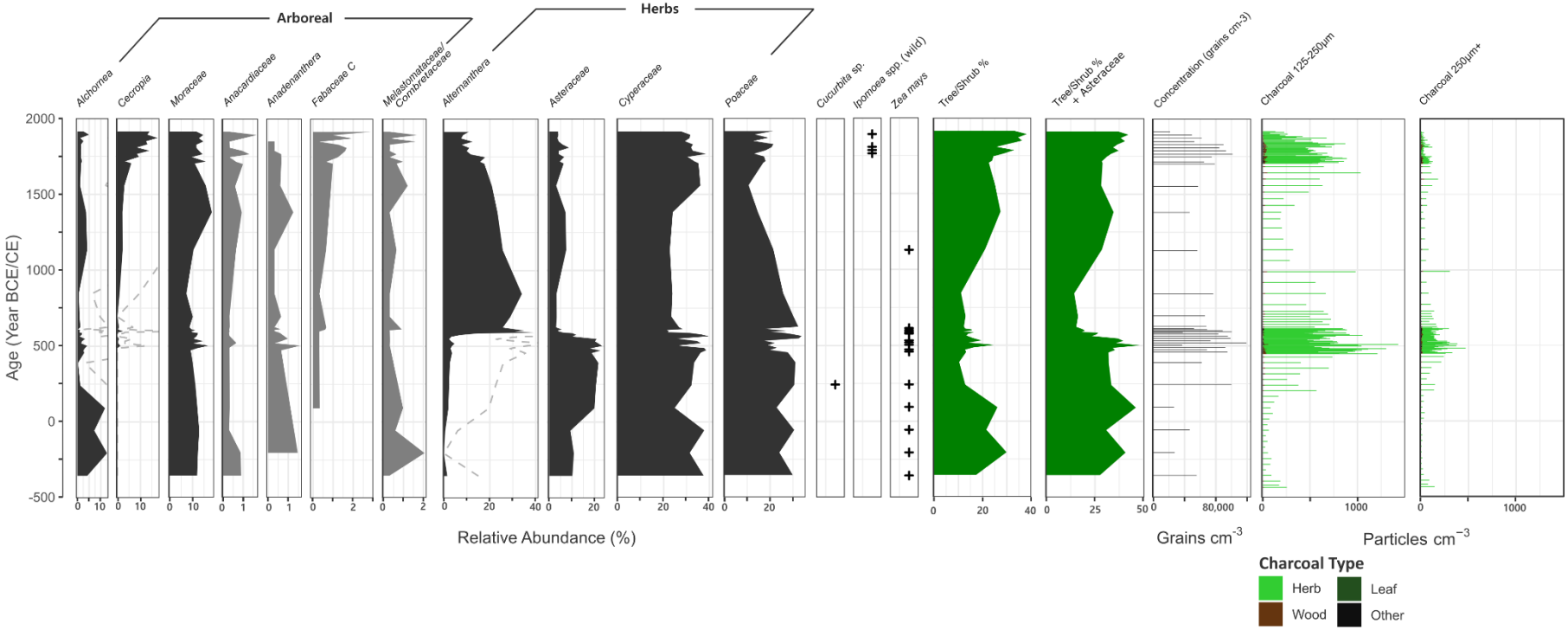

Figure S7: Summary pollen percentage diagram for LLS plotted against age, alongside charcoal data. Crosses denote presence/absence of cultigen pollen grains of Zea mays, Cucurbita and Ipomoea sp., which have been concentrated using the methodology of Whitney et al. (2012). *Dashed curves denote x10 exaggerations of certain key pollen taxa.*

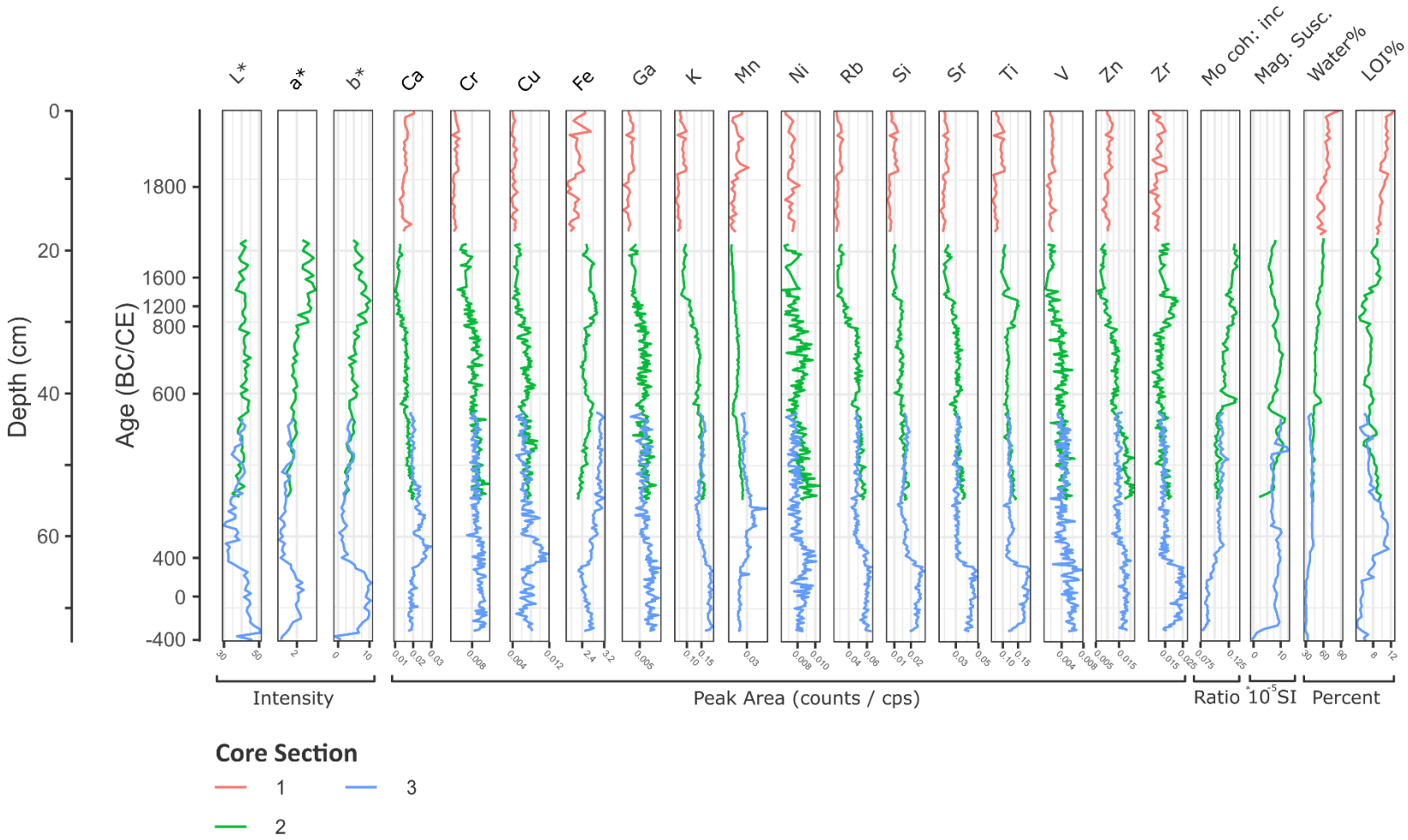

*Figure S8: XRF values for significant elements from LLS plotted against depth, expressed relative to counts per second (cps). This is combined with L*a*b* colour, magnetic susceptibility, and Water/LOI% data. This record excludes the 7cm section considered modern. Data has been mass corrected. Colour denotes core section: Blue = Livingstone Core, Green = Surface Core, Red = Surface Core Sample Vials.*

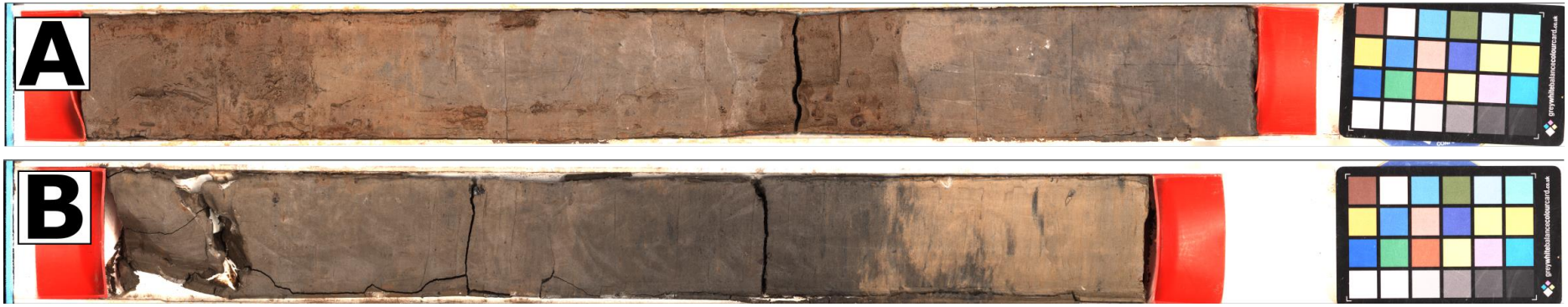

Figure S9: High Resolution photographs for the cores from LLS. (A) Surface core (18-62 cm) and (B) overlapping Livingston core (42-82 cm)

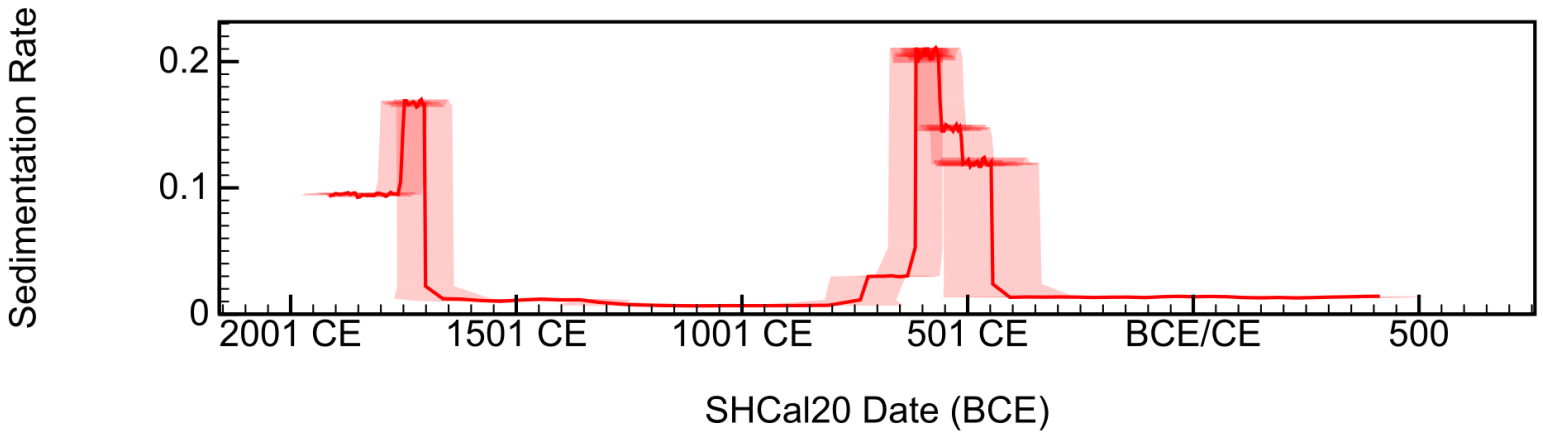

Fig S10: Sedimentation rate for LLS. This is based on the Bayesian age-depth model excluding the 7 cm sedimentary unit described in the main text.

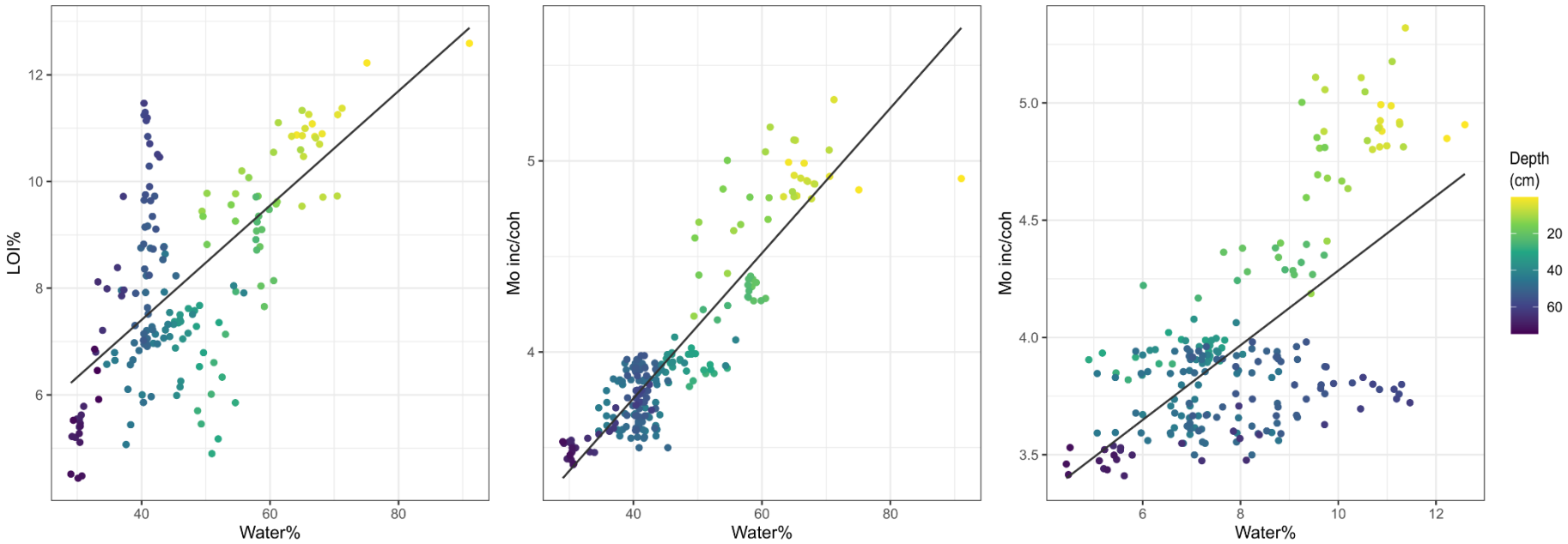

Figure S11: the Molybdenum incoherent: Coherent scattering ratio at LLS, plotted against sample water and LOI content. The former was linearly interpolated to provide measurements at depths equivalent to LOI/Water samples.

References

Bronk Ramsey, C. (2009), “Bayesian analysis of radiocarbon dates”, *Radiocarbon*, Vol. 51 No. 1, pp. 337–360.

Hogg, A., Heaton, T., Hua, Q., Palmer, J., Turney, C., Southon, J., Bayliss, A., *et al.* (2020), “SHCal20 Southern Hemisphere Calibration, 0-55,000 Years Cal BP”, *Radiocarbon*, Vol. 62 No. 4, pp. 759–778, doi: 10.1017/RDC.2020.59.

Libera, M.E. Della, Novello, V.F., Cruz, F.W., Orrison, R., Vuille, M., Maezumi, S.Y., de Souza, J., *et al.* (2022), “Paleoclimatic and paleoenvironmental changes in Amazonian lowlands over the last three millennia”, *Quaternary Science Reviews*, Elsevier Ltd, Vol. 279, p. 107383, doi: 10.1016/j.quascirev.2022.107383.

Rogerson, M., Rohling, E.J., Lourens, L.J. and Murray, J.W. (2006), “Colour Logging as a Tool in High Resolution”, *Geological Society, London Special Publications*, Vol. 1, pp. 99–112.

Whitney, B., Rushton, E., Carson, J., Iriarte, J. and Mayle, F. (2012), “An improved methodology for the recovery of Zea mays and other large crop pollen, with implications for environmental archaeology in the Neotropics”, *Holocene*, Vol. 22 No. 10, pp. 1087–1096, doi: 10.1177/0959683612441842.